SUPPORTING INFORMATION

Self-Template Impregnated Silver Nanoparticles in Coordination Polymer Gel: Photocatalytic CO_2 Reduction, CO_2 Fixation, and Antibacterial Activity

*Noohul Alam,[a] Sumit Mondal,[a] Niwesh Ojha,[b] Subham Sahoo,[a] Mohammad Tarique Zeyad,[c] Sushant Kumar[b] and Debajit Sarma[a]**

[a]Solid State and Inorganic Chemistry Group, Department of Chemistry, Indian Institute of Technology Patna, Bihar 801106, India, *E-mail: debajit@iitp.ac.in

[b]Gas-solid Interaction Laboratory, Department of Chemical and Biochemical Engineering, Indian Institute of Technology Patna, Bihar 801106, India

[c]Department of Agricultural Microbiology, Faculty of Agricultural Science, Aligarh Muslim University, Aligarh, India

Figure S1. Dynamic angular frequency sweep vs. gain modulus (G′) and loss modulus (G″) of **Ag@GMP** gel……S7
Figure S2. (a) FTIR, (b) DRS analysis of the GMP and Ag@GMP..... S8
Figure S3. The powder X-ray diffraction pattern of **Ag@GMP**, GMP and reported Ag (ICSD No. 22434).....S8
Figure S4. The particle size distribution of **Ag@GMP** from TEM image S9
Figure S5. (a) XPS survey of **Ag@GMP**, and (b) the deconvoluted peaks of Ag 3d.....S9
Figure S6. CO_2-TPD analysis of **Ag@GMP** xerogel**.**.....S10
Figure S7. Zeta potential plot of **Ag@GMP** xerogel. S10
Figure S8. UV−vis absorption spectra of (a) **Ag@GMP** xerogel, and Tuac's plots (inset) for **Ag@GMP**. S11
Figure S9. The gas chromatograph for 200 ppm CH_4 present in the standard gas mixture (composition: O_2, H_2, CO and CH_4: 200 ppm each and the rest is argon), (b) Gas chromatograph for various set of controlled/blank measurement. S11
Figure S10. The powder X-ray diffraction pattern of Ag@GMP before and after catalysis…..S12
Figure S11. ^{1}H NMR ($CDCl_3$, 500 MHz) spectra for the cycloaddition reaction of propylene oxide with CO_2 using **Ag@GMP** as catalyst. S13
Figure S12. ^{1}H NMR ($CDCl_3$, 500 MHz) spectra for the cycloaddition reaction of butylene oxide with CO_2 using **Ag@GMP** as catalyst. S13
Figure S13. ^{1}H NMR ($CDCl_3$, 500 MHz) spectra for the cycloaddition reaction of styrene oxide with CO_2 using **Ag@GMP** as catalyst. S14
Figure S14. SEM images showing the effect of **Ag@GMP** on the biofilm formation of test pathogens. (a) Control P. aeruginosa PAO1; (b) P. aeruginosa PAO1 treated with **Ag@GMP** (64 μg/ml); (c) Control S. aureus MTCC 3160; (d) S. aureus MTCC 3160 treated with Ag@GMP (64 μg/ml). S15
Table S1. Comparison table of light-driven photocatalytic CO_2 reduction with some of the reported benchmark catalysts……..S17
Table S2. Comparison of the activity of heterogeneous catalysts with those of the catalysts reported for CO_2 cycloaddition with epichlorohydrine…… S18

Experimental section

Material used. Silver nitrate hexahydrate, and guanosine 5′-monophosphate were purchased from Central Drug House (CDH). Ethanol and nafion solution (5% w/w in water) were bought from Merck and Alfa Aesar, respectively. Epichlorohydrine was brought from Sigma-Aldrich. Styrene oxide, 1,2-epoxybutane, propyleneoxide, and 1,2-epoxydecane were purchased from TCI Chemicals.

Synthesis of Ag@GMP coordination polymer gel. Typically, a 0.5 M solution of Guanosine 5′-monophosphate (GMP) and a 0.25 M solution of silver nitrate were prepared in water. Subsequently, both solutions were mixed in equal amounts. Upon stirring, the mixed solution immediately transformed into a turbid suspension. After 15 minutes, the turbid suspension was centrifuged for 5 minutes at 5000 rpm to obtain a stable coordination polymer gel (CPG). The obtained gel was dried by lyophilization. The dried form of CPG was then dispersed in an excess amount of water and stirred under condensation conditions at 90 ºC for 24 hours to remove any excess unreacted reactant. After that, the obtained material (**Ag@GMP**) was washed again with water and dried under vacuum for further characterization.

Characterization. X-ray powder diffraction (PXRD) measurement was recorded by Empyrean, Malvern Panalytical diffractometer (with Cu Kα radiation, λ = 1.5418 Å). The microstructure pattern of the **Ag@GMP** was studied by the ZEISS GEMINISem500 field emission scanning electron microscope coupled with the EDX spectroscopy detector. The JEOL- JEM-F200 transmission electron microscope operating at 200kV was also utilized to further examine the microstructure pattern of synthesized xerogel. Atomic force microscope (Agilent Technology 5500) in noncontact mode by silicon tip was used for topographical analysis. The rheological analysis was executed by Anton Paar (MCR 302) modulated compact rheometer. The storage modulus (G') and loss modulus (G") of **Ag@GMP** gel was scanned at room temperature from 0.1 to 100 rad/sec at 0.1 % strain on a nine-millimetre diameter parallel plate. FTIR spectra were recorded with the help of PerkinElmer spectrum 400 from 4000 to 500 cm^{-1} range in ATR mode. The UV-vis spectra were recorded by Shimadzu UV2500 spectrophotometer. NETZSCHSTA 449F3 instruments was used for thermogravimetric analysis at a scan rate of 20 °C/min under N_2 atmosphere.

Photoelectrochemical measurements. To perform the photoelectrochemical study, the working electrodes were fabricated by making a thin film of the as-synthesized **Ag@GMP** catalysts on FTO glass substrate (1*2 cm^2). Briefly, 20 mg of **Ag@GMP** was mixed with 2 mL of absolute ethanol and 20 µL Nafion solution to form a slurry. The doctor-blade method was used to make a thin film of the catalysts on the precleaned FTO glass and kept for drying at 70 °C for an hour. Afterwards, a 100 mL quartz cell containing 0.1 M Na_2SO_4 (pH = 7, 80 mL) with a Teflon top was utilized to assemble the three-electrode setup. The coated FTO glass acts as a working electrode, Pt wire as a counter electrode and Ag/AgCl as the reference electrode. Then, the photo-transient response was recorded by using 300 W Xe lamp (Sciencetech, Canada) under the constant bias of 0.2 V.

Gas-phase CO_2 reduction. We tested the effectiveness of the as-synthesized **Ag@GMP** catalyst by conducting gas-phase photoreduction of CO_2 in the presence of photocatalyst, moisture, and light, without using any sacrificial agent. First, we dispersed 50 mg of the catalyst in 10 mL of Milli-Q water and sonicated the mixture for 30 minutes. Then, we directly poured the solution onto the concave surface of a two-necked quartz glass and left it in the oven at 80 °C overnight to dry. This process resulted in the formation of a uniform thin film of catalyst on the concave wall of the reactor.

To create a closed system, we sealed the two apertures of the reactor with silicone rubber septa. We continuously passed ultrapure carbon dioxide gas through the system to prevent contamination with oxygen, periodically opening and closing valves to vent off any unwanted gas. Meanwhile, we used a gas chromatograph (GC) (Centurion Scientific, Model-5800) to monitor the gas composition inside the quartz reactor, injecting a 1 mL gas-tight Hamilton syringe regularly.

Once the reactor was free of oxygen, we circulated ultrapure carbon dioxide gas through a Milli-Q water bubbler for 30 minutes at room temperature. The gas flow rate was maintained at 5 mL/min using a mass flow controller (Aalborg Instruments, USA). Additionally, we added 15 µL of Milli-Q water to the reactor and heated it to 80 °C for 15 minutes before bringing it back to room temperature. To ensure the adsorption-desorption equilibrium of carbon dioxide gas with the catalyst, we kept the reactor in the dark for two hours. Then, we switched on the Xe-lamp and analyzed the resulting products using gas chromatography equipped with a thermal conductivity

detector (TCD), a flame ionized detector (FID), and a methanizer. Argon served as the carrier gas, and the column material was a molecular sieve (length 5 m, ID 2.1 mm).

In situ DRIFTS study. We conducted an in-situ DRIFTS study to uncover reaction intermediates and shed light on the potential reaction mechanism involved in the photocatalytic reduction of CO_2 in the presence of water under irradiation. For that, we have used a thermo-scientific Nicolet iS50 infrared spectrometer, which consisted of the HARRICK praying Mantis reaction chamber and an MCT-A (Mercury Cadmium Telluride) detector cooled by liquid nitrogen. Into the chamber, we loaded about 5 mg of catalysts mixed with KBr (1:100 w/w). To remove adsorbed species on the chamber and catalyst surfaces, we heated them to 150 °C in a vacuum for two hours, allowing the chamber to naturally cool afterwards. Then, ultrapure carbon dioxide gas flowed at a rate of 5 mL/min through a water bubbler in the Harrick cell for 30 minutes. To establish equilibrium between gaseous species and photocatalyst, we closed all inlet and outlet valves for 2 hours to form a batch system. Following this, we obtained the background spectrum. We then utilized light from a 500W Xenon arc lamp to shine through the quartz window, and data were acquired for 2 hours at regular intervals.

Bacterial strains and growth conditions. Antibacterial activity against Gram-positive and Gram-negative bacteria was determined. *Escherichia coli* ATCC 25922, *Pseudomonas aeruginosa* PAO1, *Staphylococcus aureus* MTCC 3160 and *Bacillus subtilis* were used in the study. All bacterial cultures were grown and maintained in nutrient broth (5 g/L peptone, 5 g/L NaCl, 1.5 g/L beef extract and 1.5 g/L yeast extract) at 37 ℃. The experiments were also carried out in nutrient broth at the same temperature. The agar-well diffusion method was used to determine the susceptibility of the test microorganisms to complex (Bauer et al., 1996). 100 µL overnight grown bacterial cells were spread on Nutrient agar plates. The plates were punched with 8 mm wells, 20 µL of the test complex were added, and the plates were incubated at 37 °C. By measuring the halo zones surrounding the wells, the antibacterial activity was measured.

The minimum inhibitory concentration (MIC) of test compounds against each of the bacteria was determined using the micro-broth dilution method, with doses tested ranging from 512 to 8 µg/mL. Using a macro-broth dilution approach, MBC was evaluated against all test

pathogens. Overnight-grown cultures of bacteria from each treated concentration were streaked on nutrient agar plates to determine MBC (*Dakal et al., Front Microbiol. 2016 Nov 16;7:18*31).

Inhibition of Biofilms. Biofilm inhibition was visually validated by growing biofilms on glass coverslips and viewing them using light, confocal laser scanning microscopy (CLSM) and scanning electron microscopy (SEM) (Qais et al., 2019)

Light microscopy. The bacterial strains were grown on 24 well tissue culture plates with and without 64 µg/mL complex. Sterile glass coverslips of 1 × 1 cm size were put in each well in a slant position and incubated for 24 hours at their respective optimal temperatures under static conditions. After incubation, the glass coverslips were gently washed with sterile phosphate buffer to remove any loosely attached cells. A few drops of 0.1% (w/v) crystal violet solution were used to stain the biofilms on the glass surface for 15 minutes. The excess stain was washed away with sterile phosphate buffer and allowed to dry at room temperature. The biofilms were imaged at 40X magnification using a light microscope (Olympus BX60, model BX60F5, Olympus Optical Co. Ltd. Japan) equipped with a colour VGA camera (Sony, model no. SSCDC-58AP, Japan).

CLS Microscopy. As previously stated, the biofilms were formed on a glass surface for confocal imaging. The glass coverslips were withdrawn and thoroughly washed with sterile phosphate buffer. The biofilms were stained for 20 min using 0.1% acridine orange followed by repeated washing to remove excess stain. The glass coverslips were air-dried in the dark at room temperature and images were captured at 63X magnification with a Zeiss LSM780.

Scanning electron microscopy. As explained above, biofilm was formed on coverslips for scanning electron microscopic examination. The slides were dehydrated using ethanol gradient (20–100%) and fixed in glutaraldehyde. Coverslips were coated with gold and visualized under JEOL-JSM 6510 LV (Qais et al., 2020).

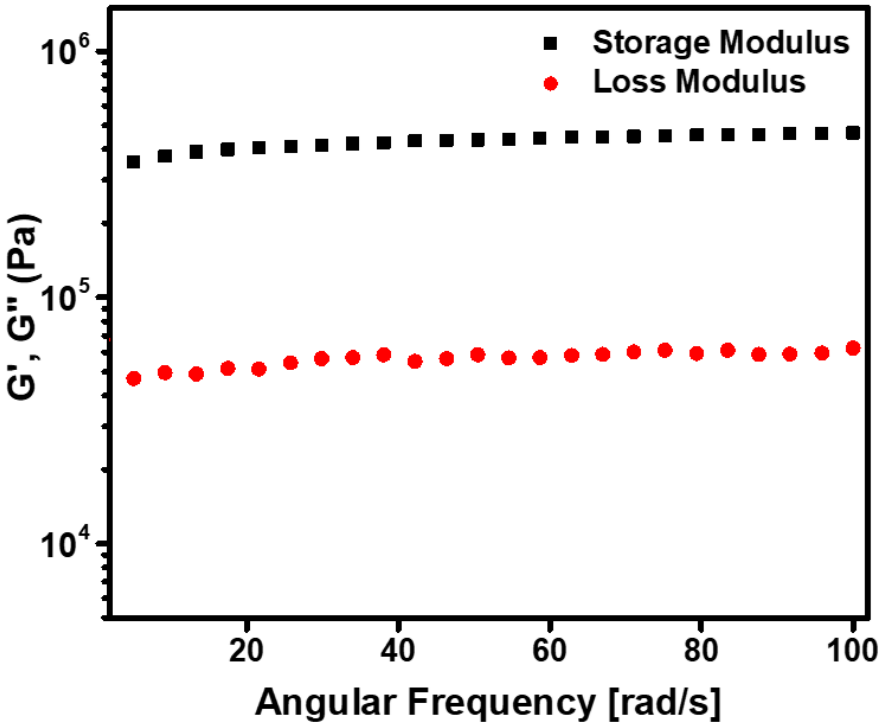

Figure S1. Dynamic angular frequency sweep vs. gain modulus (G′) and loss modulus (G″) analysis was performed to check the viscoelastic nature of the as synthesized **Ag@GMP** gel. For any gel material, the value of storage modulus (G′) must be higher than the loss modulus (G″). The figure demontarte that the G' and G" values were remained almost constant in the entire test region and did not cross to each other (i.e, G'> 10^5, G"<10^5), confirming the gel nature of the material.

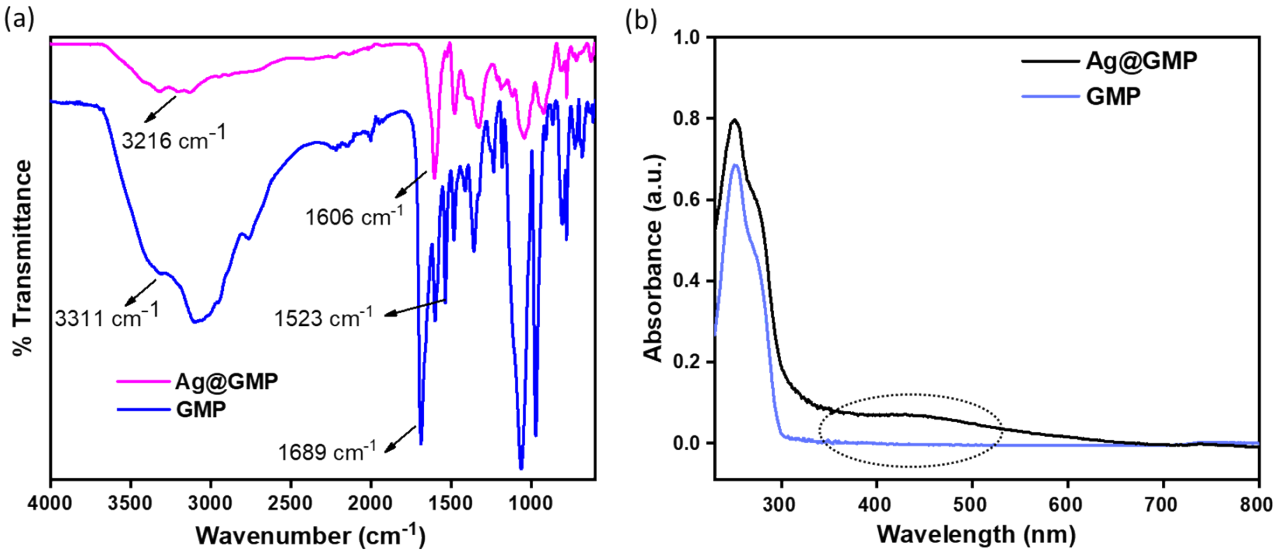

Figure S2. (a) FTIR, (b) DRS analysis of the GMP and Ag@GMP.

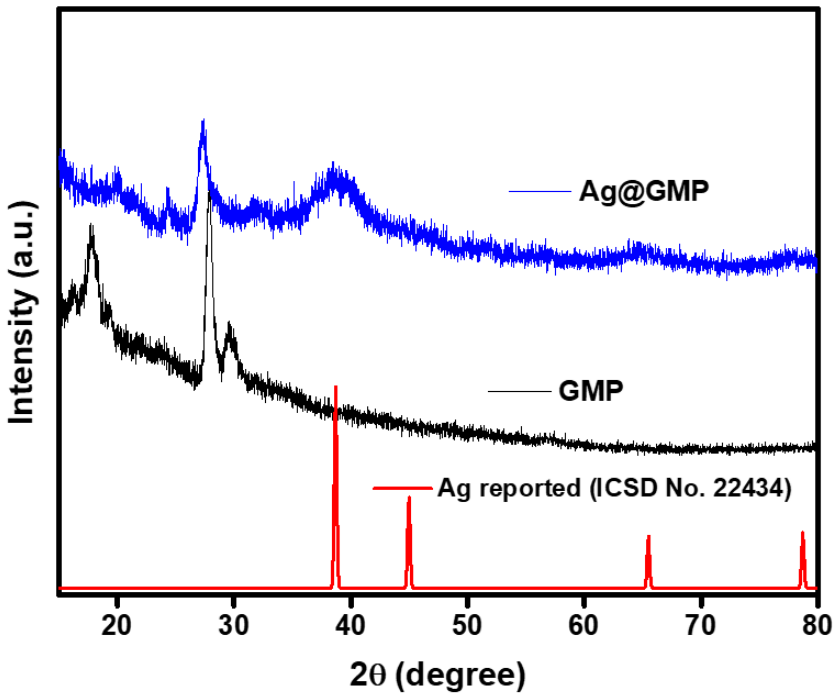

Figure S3. The powder X-ray diffraction pattern of **Ag@GMP**, GMP and reported Ag (ICSD No. 22434).

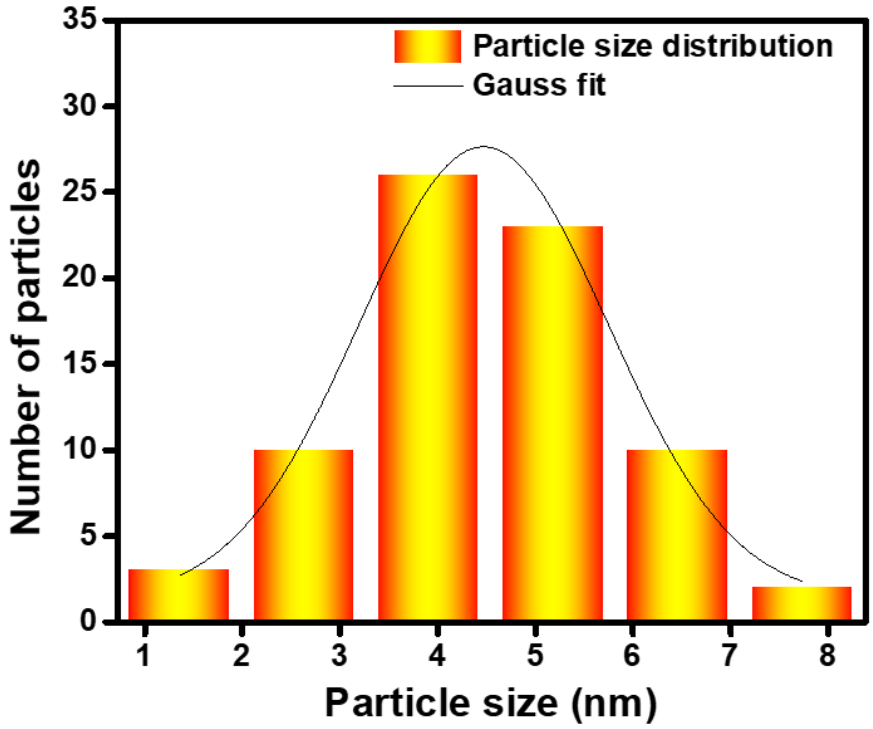

Figure S4. The particle size distribution of **Ag@GMP** from TEM image.

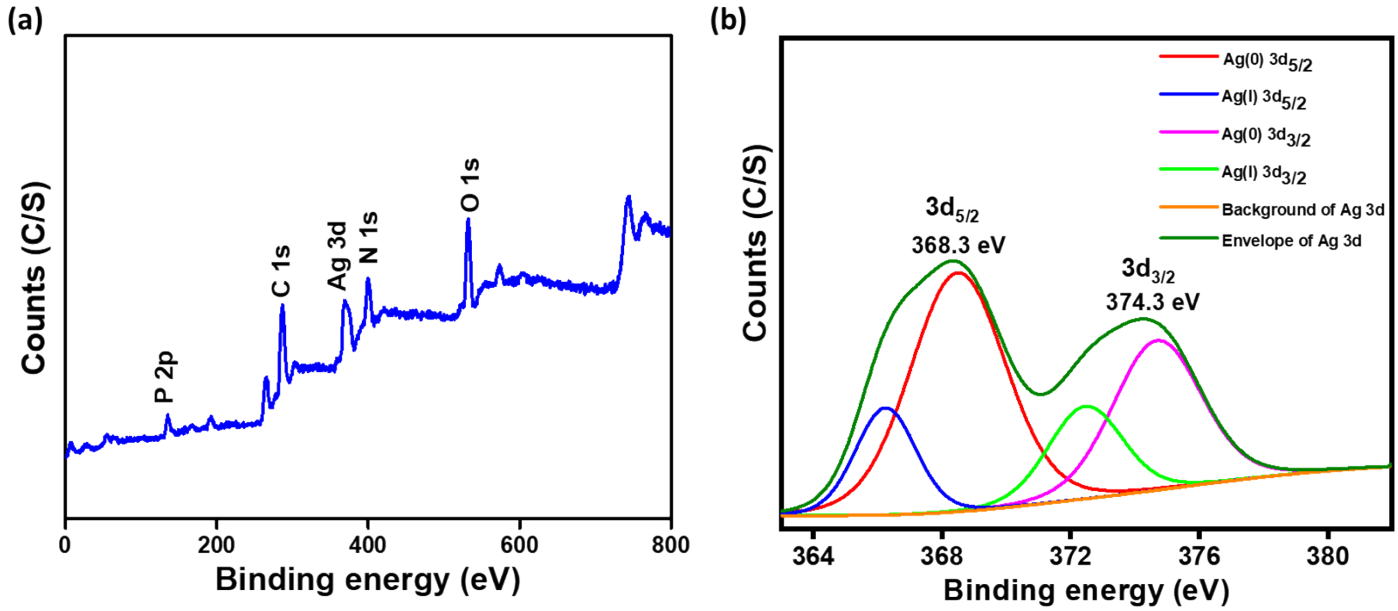

Figure S5. (a) XPS survey of **Ag@GMP**, and (b) the deconvoluted peaks of Ag 3d.

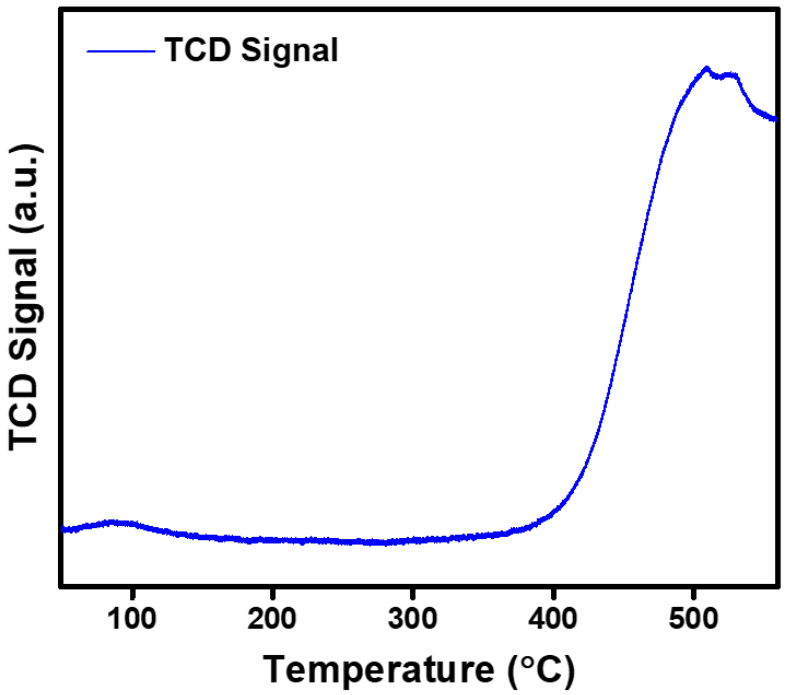

Figure S6. CO_2-TPD analysis of **Ag@GMP** xerogel**.**

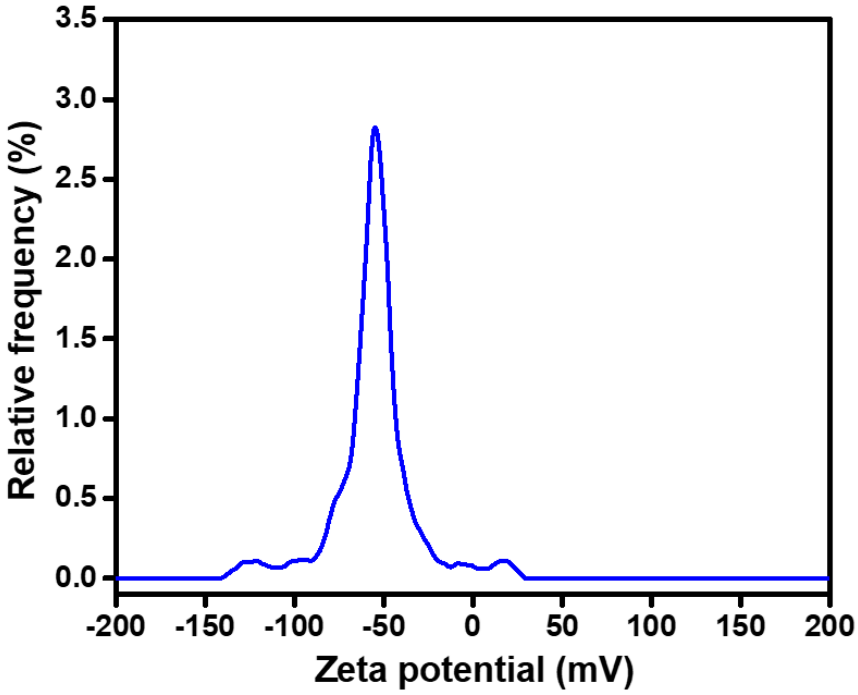

Figure S7. Zeta potential plot of **Ag@GMP** xerogel.

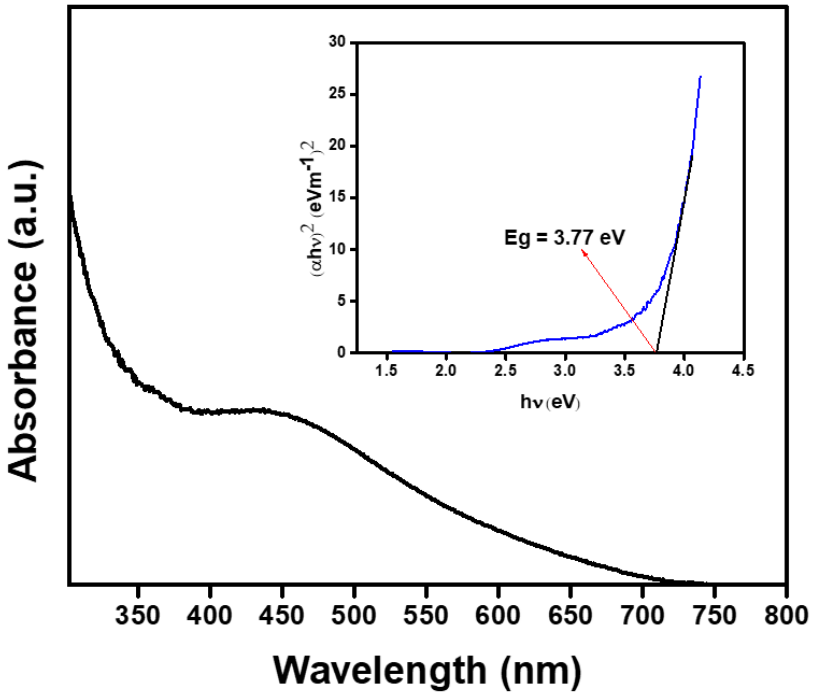

Figure S8. UV−vis absorption spectra of (a) **Ag@GMP** xerogel, and Tuac's plots (inset) for **Ag@GMP**.

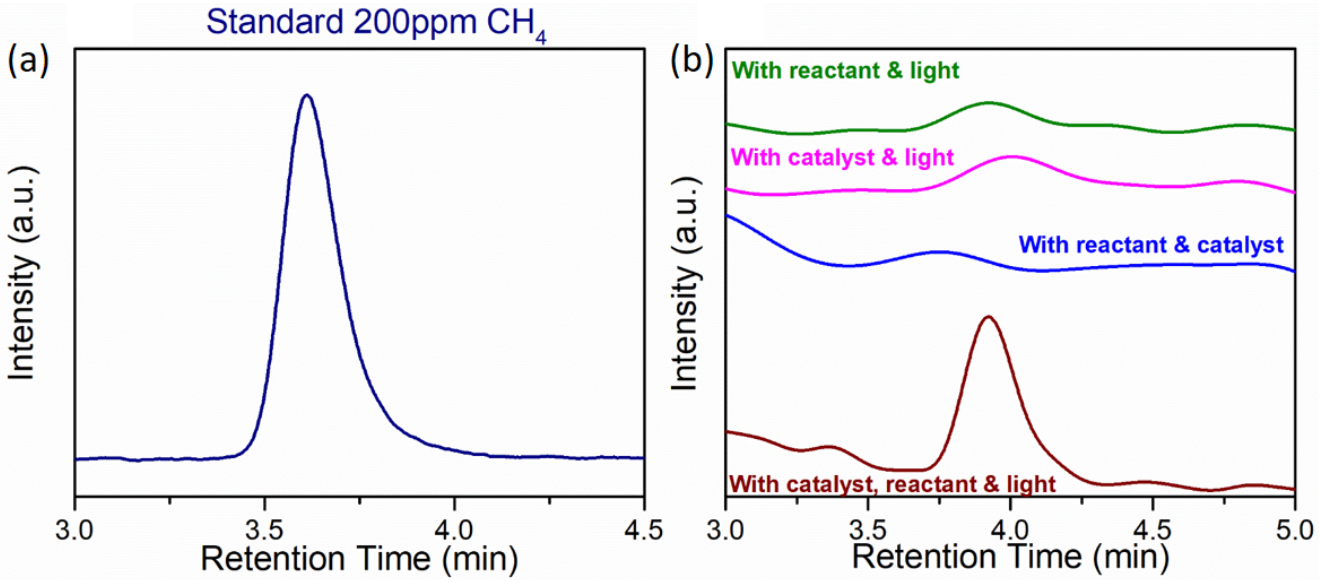

Figure S9. The gas chromatograph for 200 ppm CH_4 present in the standard gas mixture (composition: O_2, H_2, CO and CH_4: 200 ppm each and the rest is argon), (b) Gas chromatograph for various sets of controlled/blank measurements.

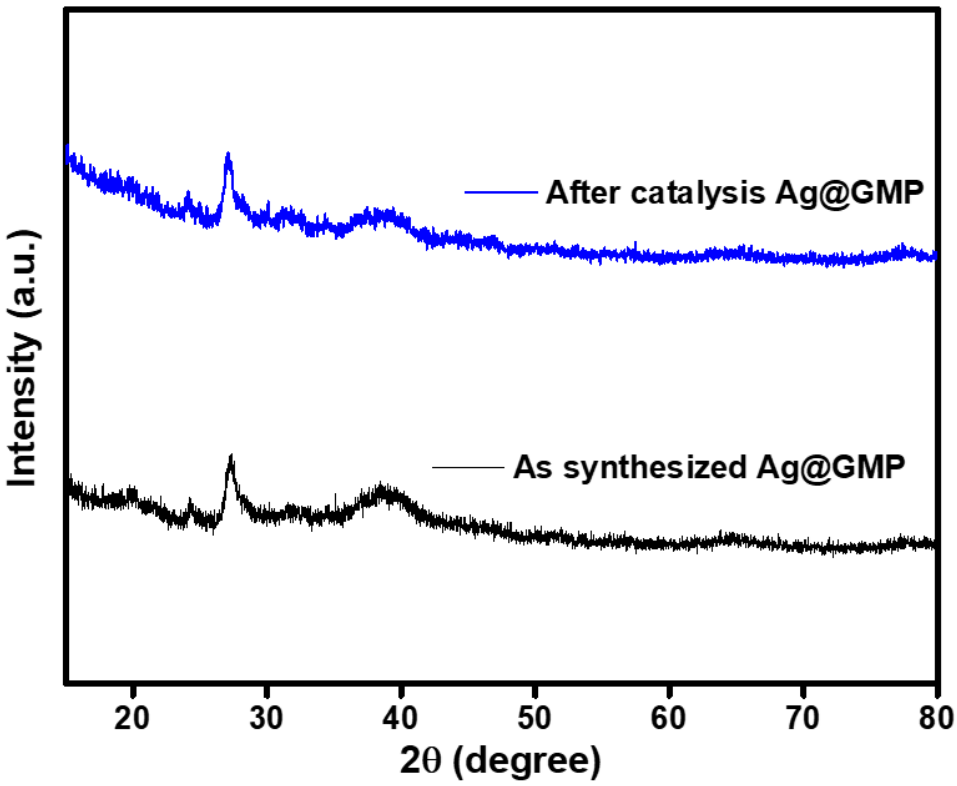

Figure S10. The powder X-ray diffraction pattern of Ag@GMP before and after catalysis.

[1]H-NMR analysis of the substrate scopes (CO_2 cycloaddition).

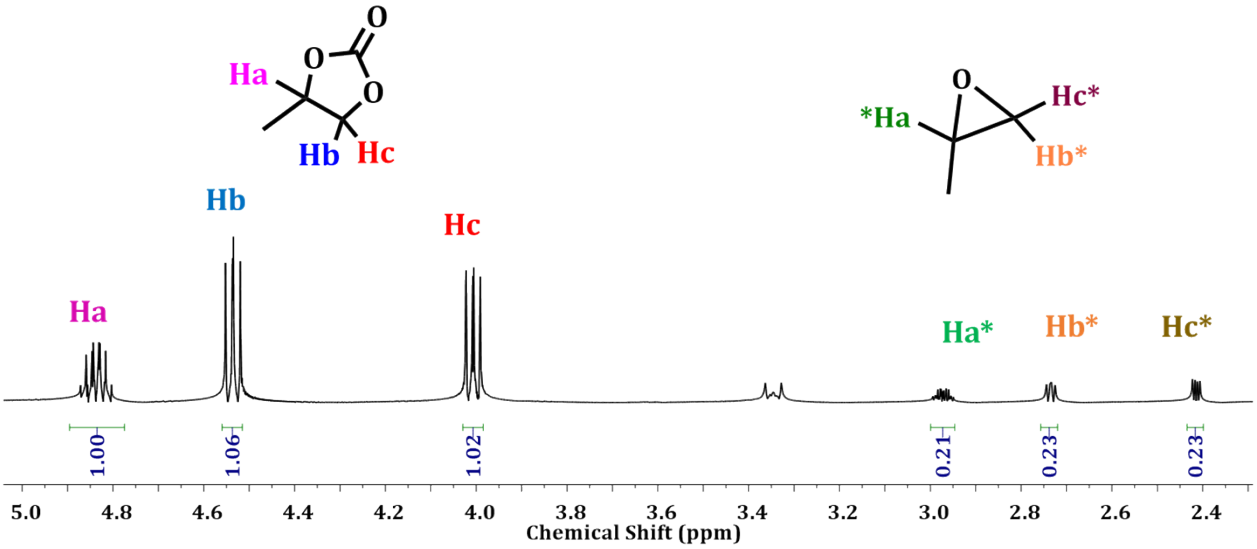

Figure S11. [1]H NMR ($CDCl_3$, 500 MHz) spectra for the cycloaddition reaction of propylene oxide with CO_2 using **Ag@GMP** as a catalyst.

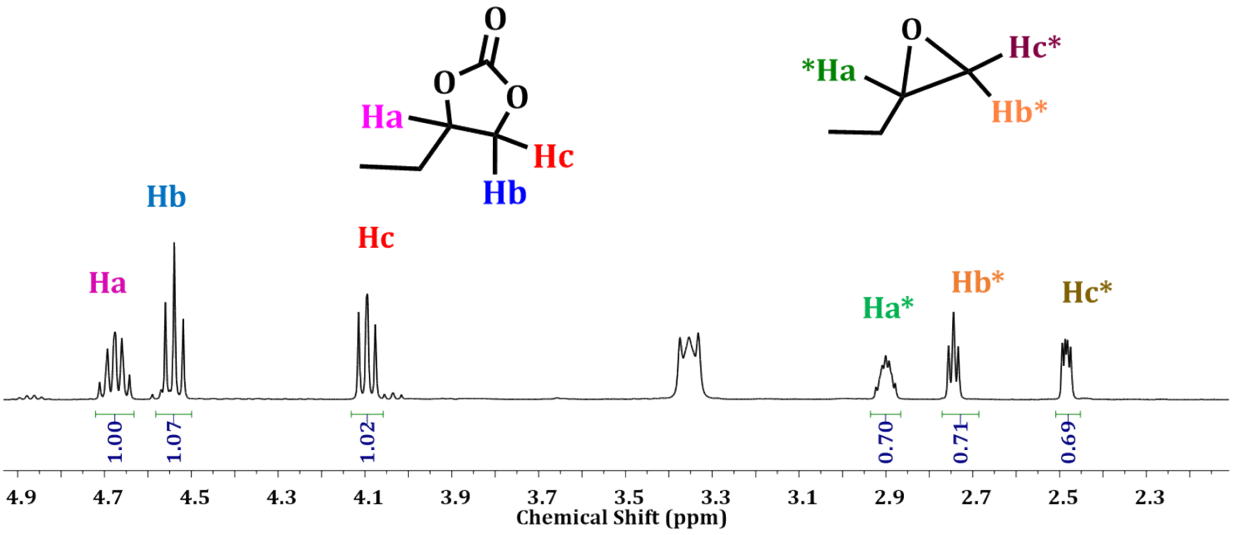

Figure S12. [1]H NMR ($CDCl_3$, 500 MHz) spectra for the cycloaddition reaction of butylene oxide with CO_2 using **Ag@GMP** as a catalyst.

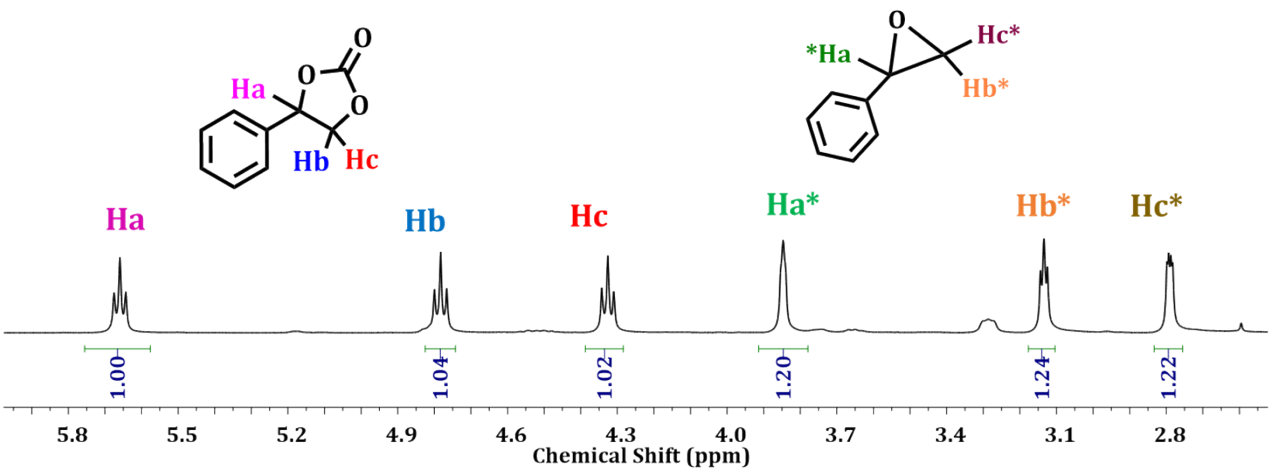

Figure S13. ^{1}H NMR ($CDCl_3$, 500 MHz) spectra for the cycloaddition reaction of styrene oxide with CO_2 using **Ag@GMP** as a catalyst.

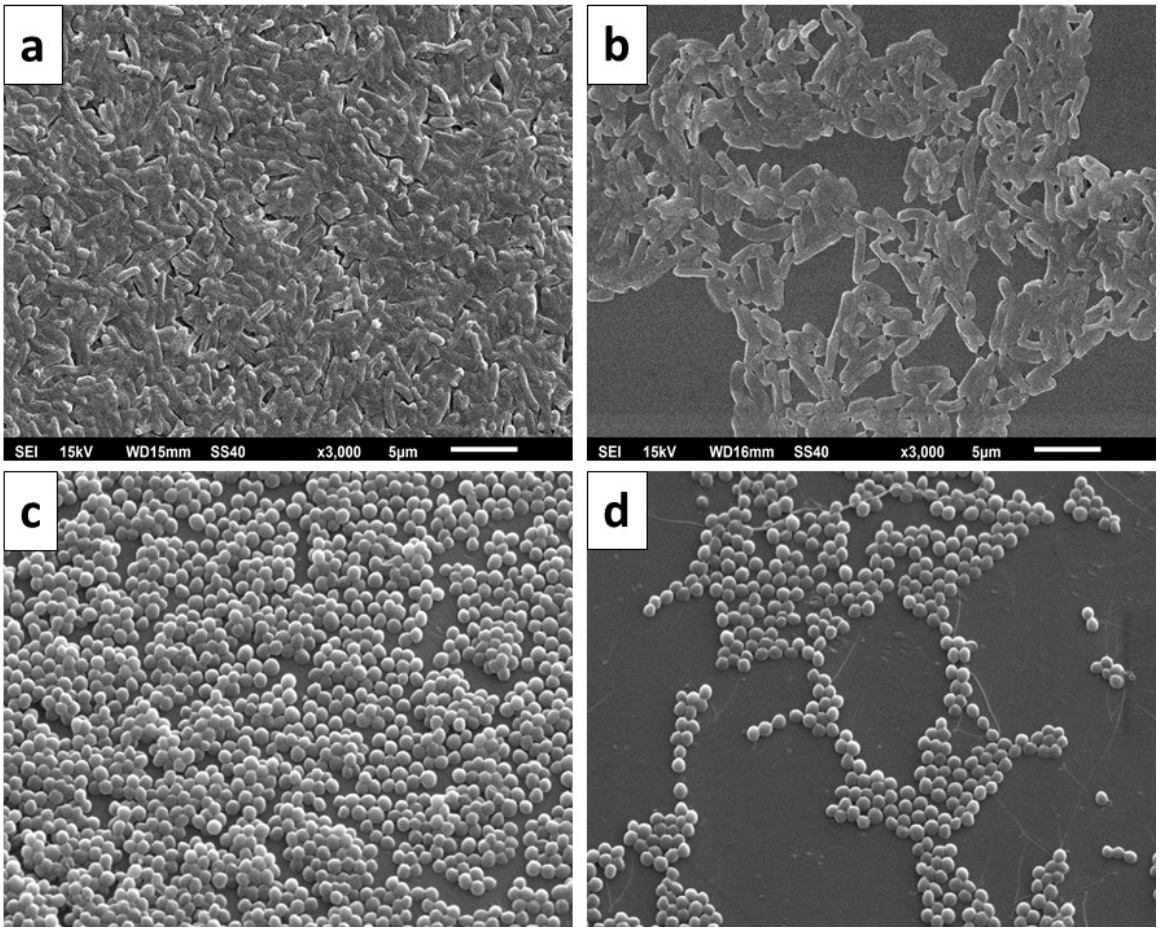

Figure S14. SEM images showing the effect of **Ag@GMP** on the biofilm formation of test pathogens. (a) Control *P. aeruginosa PAO1*; (b) *P. aeruginosa PAO1* treated with **Ag@GMP** (64 µg/mL); (c) Control *S. aureus MTCC 3160*; (d) *S. aureus MTCC 3160* treated with Ag@GMP (64 µg/mL).

Intermediate steps in photocatalytic CO_2 reduction.

$$Catalyst + h\nu \rightarrow e_{CB}^{-} + h_{VB}^{+} \quad \text{(R1)}$$

$$CO_2 + e^{-} \rightarrow CO_2^{-} \quad \text{(R2)}$$

$$H_2O + h_{VB}^{+} \rightarrow H^{+} + OH^{\bullet} \quad \text{(R3)}$$

$$OH^{\bullet} + CO_2^{-} \rightarrow HCO_3^{-} \quad \text{(R4)}$$

$$CO_2^{-} + CO_2^{-} \rightarrow CO + CO_3^{2-} \quad \text{(R5)}$$

$$CO_2^{-} + H^{+} + e^{-} \rightarrow CO + OH^{-} \quad \text{(R6)}$$

$$HCO_3^{-} + H^{+} + e^{-} \rightarrow CO + 2OH^{-} \quad \text{(R7)}$$

$$CO_3^{2-} + 2H^{+} + 2e^{-} \rightarrow CO + 2OH^{-} \quad \text{(R8)}$$

$$CO_2 + 2H^{+} + 2e^{-} \rightarrow HCOOH \quad \text{(R9)}$$

$$CO_2 + 8\,H^{+} + 8e^{-} \rightarrow CH_4 + 2H_2O \quad \text{(R10)}$$

Table S1. Comparison table of light-driven photocatalytic CO_2 reduction with some of the reported benchmark catalysts.

Material names	Product yield ($\mu mol\ h^{-1}\ g^{-1}$)	Reaction Conditions	Sacrificial agents	Ref.
MIL-101-Cr	8.3	CO_2/H_2O/TEOA	TEOA	[1]
(CoPPc)/ (mpg-CNx)	18.75	CO_2/CH_3CN/TEOA	TEOA	[2]
Ni-Complex PS: $[Ru(bpy)_3]\ Cl_2$	10.2	CO_2/DMA, H_2O/ BIH	Mg^{2+}	[3]
NiCoOP NPs/ $[Ru(bpy)_3]Cl_2 \cdot 6H2O$	16.6	CO_2/CH_3CN/TEOA	TEOA	[4]
Ptn/3 DOMSrTiO_3	4.1	CO_2/H_2O	--	[5]
ZnPorphyrinTTF-COF (TTCOF-Zn)	2.05	CO_2/H_2O	--	[6]
MF@NCA	1.4	CO_2/H_2O	No sacrificial agent	[7]
$Zn_{0.4}Ca_{0.6}In_2S_4$	0.224	CO_2	--	[8]
Ag@GMP	**1.55**	**CO_2/H_2O, at ambient condition**	**Without any sacrificial agent**	**This work**

Table S2. Comparison of the activity of heterogeneous catalysts with those of the catalysts reported for CO_2 cycloaddition with epichlorohydrine.

Catalyst	Time (h)	Temperature (^oC)	Pressure (bar)	Conversion (%)	Ref.
Cu(II)-MOG	48	RT	1	80	[9]
MOG	48	RT	1	78	[10]
NiXero	9	80	5	45	[11]
UMCM-1-NH_2	24	RT	12	78	[12]
MOF-5	12	RT	6	93	[13]
Zn-DAT	24	RT	8	99	[14]
COF-PI-2	24	RT	1	99	[15]
Eu-MOF	4	80	1	99	[16]
Cu-K-MOF	18	60	1	99	[17]
SSICG-3	12	RT	1	99	[18]
Ag@GMP	**48**	**RT**	**1**	**99**	**This work**

References:

1. Y. Xie, Z. Fang, L. Li, H. Yang and T.-F. Liu, *ACS Appl. Mater. Interfaces*, 2019, **11**, 27017-27023.
2. S. Roy and E. Reisner, *Angew. Chem. Int. Ed.*, 2019, **58**, 12180-12184.
3. D. Hong, T. Kawanishi, Y. Tsukakoshi, H. Kotani, T. Ishizuka and T. Kojima, *J. Am. Chem. Soc.*, 2019, **141**, 20309-20317.
4. Y. Wang, S. Wang and X. W. Lou, *Angew. Chem. Int. Ed.*, 2019, **58**, 17236-17240.
5. X. Wu, C. Wang, Y. Wei, J. Xiong, Y. Zhao, Z. Zhao, J. Liu and J. Li, *J. Catal.*, 2019, **377**, 309-321.
6. M. Lu, J. Liu, Q. Li, M. Zhang, M. Liu, J. L. Wang, D. Q. Yuan and Y. Q. Lan, *Angew. Chem.*, 2019, **131**, 12522-12527.
7. N. Alam, N. Ojha, S. Kumar and D. Sarma, *ACS Sustain. Chem. Eng.*, 2023, **11**, 2658-2669.
8. C. Zeng, H. Huang, T. Zhang, F. Dong, Y. Zhang and Y. Hu, *ACS Appl. Mater. Interfaces*, 2017, **9**, 27773-27783.
9. C. K. Karan, M. C. Sau and M. Bhattacharjee, *Chem. Commun*, 2017, **53**, 1526-1529.
10. C. K. Karan and M. Bhattacharjee, *Eur. J. Inorg. Chem.*, 2019, **2019**, 3605-3611.
11. E. Saha, H. Jungi, S. Dabas, A. Mathew, R. Kuniyil, S. Subramanian and J. Mitra, *Inorg. Chem.*, 2023, **62**, 14959-14970.
12. R. Babu, A. C. Kathalikkattil, R. Roshan, J. Tharun, D.-W. Kim and D.-W. Park, *Green Chem.*, 2016, **18**, 232-242.
13. J. Song, Z. Zhang, S. Hu, T. Wu, T. Jiang and B. Han, *Green Chem.*, 2009, **11**, 1031-1036.
14. R. Das, S. S. Dhankhar and C. Nagaraja, *Inorg. Chem. Front.*, 2020, **7**, 72-81.
15. L.-G. Ding, B.-J. Yao, W.-X. Wu, Z.-G. Yu, X.-Y. Wang, J.-L. Kan and Y.-B. Dong, *Inorg. Chem.*, 2021, **60**, 12591-12601.
16. M. Sinchow, N. Semakul, T. Konno and A. Rujiwatra, *ACS Sustain. Chem. Eng.*, 2021, **9**, 8581-8591.
17. Y. Yang, C. Tu, J. Shi, X. Yang, J.-J. Liu and F. Cheng, *Cryst. Growth Des.*, 2022, **22**, 4813-4820.
18. S. Sahoo and D. Sarma, *Cryst. Growth Des.*, 2022, DOI: 10.1021/acs.cgd.2c00737.